A Simplified Model of Surface Burnishing and Friction in Repeated Make-up Process of Premium Tubular Connections

H. R. Le[1]*, F. Stewart[2], J. A. Williams[3]

[1]School of Marine Science and Engineering, Plymouth University, Plymouth, UK

[2]DNV GL, Aberdeen, UK

[3]Department of Engineering, University of Cambridge, Cambridge, UK

*Corresponding author (*H. R. Le): +44 1752 586100* (huirong.le@plymouth.ac.uk)

Abstract

We develop a simplified model to predict the frictional behaviour of the contact between the surfaces of a rotary shouldered thread connection in the make-up process of premium tubular connections as used in the oil pipeline business. A classic wear model is applied at the scale of the surface asperities to predict the evolution of friction between initially shot-peened surface and bronze plated surface in repeated sliding. Validation is provided by experimental measurements of surface roughness before and after sliding. An average friction model is developed by applying a friction factor model to the asperity contact areas and an Eyring shearing theory to the entrapped thin lubricant film. The predictions of the magnitude of friction over various sliding cycles are compared with measurements from physical tests.

Keywords: Threaded connection; Surface burnishing; Sliding friction; Micromechanical modelling

NOMENCLATURE

a	contact patch radius	H_t	ratio $h_t : R_a$
a_2, a_3	constants	H_{tc}	critical value of H_t
c	boundary friction factor	H_1, H_2	Vickers hardness of surface 1 and 2
d_m	mean diameter thread	P_v	fluid pressure
d_c	mean diameter shoulder	P_a	asperity pressure
h	asperity height	R	reduced radius of contact
h_t	mean oil film thickness	R_a, R_q	surface roughness parameters
k	dimensionless wear rate	$R_{q,1}, R_{q,2}, R_{qc}$	*rms surface roughness of contact*
l	thread pitch	T	torque
m	asperity geometric factor	V	volume
$\bar{p}$	mean pressure	W	normal load
p_r	shoulder pre-load	β	thread flank angle
q_x, q_s	flow rates	Λ	contact ratio
s	sliding distance	μ, μ_c	coefficients of friction
v	sliding velocity	τ	shear stress
y0	initial asperity peak to valley height	γ	Peklenik number
z	normalised surface height	η	viscosity
E^*	contact modulus	ϕ_x, ϕ_s	flow factors
F	friction or tangential force	τ_0	Eyring stress
F_N	normal load		

1 Introduction

An oil or gas pipeline can be regarded as a long pressure vessel transporting crude oil or gas from the bottom of a well to the well-head and beyond. Rotary shouldered thread

connections, also known as premium tubular connections, are commonly used to connect the pipes in well completion (1, 2). These tubular connections are increasingly exposed to harsh off-shore environments involving high temperatures and highly acidic conditions (3) and a small proportion of connections may fail during their working life with significant financial implications. The Wall Street Journal concluded that gas leaks in the North Sea in 2012 had cost billions of dollars through lost production, replacement of connections and unplanned well interventions (4, 5).

A premium tubular connection consists of a pair of threaded conical pipe ends and a threaded coupling as shown in Fig. 1. The final stage of the manufacturing process commonly involves shot peening the mating surfaces in order to improve fatigue life and stabilise friction during assembly. To maintain working pressures it is important that the connections are fully sealed by applying the correct torque during the make-up process so that sufficient pre-load is applied to the metal-to-metal seal at the shoulder. This has been investigated in a previous paper by the authors (6). The make-up torque T can be related to the coefficient of friction (CoF) at the interacting surfaces by the well-established equation for power screw mechanisms, eqn (1), which combines a torque component generated by the friction on the loading flank of threads with that generated by contact between the components at the shoulder (7),

$$T = \frac{p_r d_m}{2}\left(\frac{l + \pi\mu d_m \sec\beta}{\pi d_m - \mu l \sec\beta} + \mu_c \frac{d_c}{d_m}\right). \tag{1}$$

Here p_r is the pre-load on the shoulder, d_m the mean diameter of the thread, d_c the mean diameter of the shoulder, l the pitch of the thread, μ the coefficient of friction at the thread, μ_c the coefficient of friction at the collar and β the flank angle of the thread.

The current procedure favoured by the Oil Country Tubular Goods (OCTG) industry is to determine a value of torque for each pipe size using an empirical CoF value and desired pre-load on the seal. According to the API - 7G Recommended Practice (8), CoF between mating surfaces, i.e. threads and shoulders, lies in the range of 0.07 to 0.08. There is no consideration of the effects of surface finish, lubricant type and operation speed. However, it is well known that the torque versus rotation curve can change with operational conditions for a given size of pipe. If there is a significant change in the torque characteristics during operation, the operators repeat the process up to three times for each coupling before discarding the product. The same torque value would be used for the second or third time. This trial and error approach significantly increases the cost of time and waste of materials in the field.

In order to determine the coefficient of friction more accurately, connection samples are torqued until yielding so that the pre-load pressure p_r can be estimated for a given geometry of pipe end and the yield strength of the material. Due to the expense of such destructive testing it is not viable to test all combinations of sizes and grades of pipes. Extrapolation or interpolation is therefore needed to obtain torque values for the untested sizes: these can become unreliable owing to the nonlinear effects of contact pressure, operating speed and surface conditions. Although in some situations this process may cause few problems to pipelines, it may have catastrophic problems in the future when well-depths and the associated temperatures and pressures increase significantly.

The API RP 5A3 (3rd Edition) document describes a simple method for obtaining frictional data for threaded connections (9). The test set-up consists of a standard 1 inch nut engaged on a bolt which is rotated into the stationary thread until a specific pre-load is applied

to the shoulder. The CoF value is acquired using the torque data and the estimated contact pressure from the angle of relative rotation. Although this is a widely used testing procedure for new materials and lubricants, it lacks control of contact pressure and surface finish on the components. There are also uncertainties about the validity of contact conditions and lubrication regime. The contact pressure generated in this setup is of order 200 to 400 MPa (30 - 65 ksi) on the loading collar and below 260 MPa (40ksi) on the threads. This is significantly lower than the values of contact pressure on the seal and thread sections of a premium connection which, on the basis of Finite Element Analysis, have been predicted to be of the order of 700 to 2000 MPa (100 to 300ksi). The lubrication regime in API test is more likely in a mixed regime with boundary and hydrostatic lubrication. There is a much lower risk of galling in API tests than in pipe connection.

An alternative test suggested by Carper et al (10) used a conical pin and box with coincident tapers to measure the friction coefficient. The box was rotated whilst the normal load was increased linearly and the CoF was extracted from the torque applied and the axial force. To produce the necessary contact pressures, large axial forces and torques were required and this meant that a large experimental device was needed which incurs significant costs.

A much smaller cross-cylinder friction test rig was developed by the authors to simulate the contact regimes on the threads of a tubular connection (6) and is illustrated in Fig. 3. It was designed so that samples in the form either of cylinders, of radius 6 mm, or coupons, with a cylindrical surface of radius 60 mm, could be pressed together with their axes at 90°. The upper stationary sample represents the pipe end whilst the lower moving sample represents the coupling. The axis of the lower specimen is parallel to its motion so that the

contact point on the upper surface remains at rest during the test while the point of contact moves along the lower cylindrical surface. This configuration simulates the real connection system because during the make-up of the connection, the thread of the pipe is subjected to continuous sliding with the new thread of the coupling. The test can also illustrate the effect of burnishing, by repeated contact, of the top sample. The lower specimen is carried on a linear stage whose tilt can be adjusted so that the normal load between the specimens increases during the course of the test, see Fig. 3(a). Each test consisted of a number of cycles, completed consecutively. Lubricant can be reapplied between each load cycle to replicate the conditions of the real pipe connection make-up situation. Both normal force W and tangential force F were measured simultaneously using sixteen strain gauges fixed on the four legs of the specially designed load cell. This is of a similar design to the two component load cell reported previously by the authors (11, 12). The output normal and tangential voltages were filtered through their respective amplifiers and then fed into a data logging card interfaced with the PC using LabVIEW®. The coefficient of friction is simply defined as the ratio of F to W.

The test rig allowed for quick measurement of CoF under very high contact pressures and various combinations of surface roughness, surface coating, lubricant type and sliding speed. Tests were carried out with a stationary shot-peened sample against a moving plated counterface with a ramping normal force at speeds of between 3 and 50mm/s in accordance with the operational conditions of premium connections. The results indicated that with as-received surfaces the initial CoF reduced rapidly in magnitude during the first stroke and then stabilised in subsequent test cycles. This was coincident with a rapid drop in the surface roughness of the initially shot-peened surface, as reported in (6). This trend is similar to that observed in the cold drawing of shot-blasted stainless steel strips studied by Le et al (13). In

both cases, one component is subjected to shot-peening which creates crater like features on the surface. Lo and Wilson (14) and Sutcliffe et al (15) found that these craters can act as lubricant reservoirs in sliding contact. On the other hand, any large asperities around the edges of the craters increase the risk of galling and hence exacerbate friction.

In what follows we investigate surface asperity wear during sliding and develop a simplified friction model that reflects the contact and lubrication regimes for the metal-to-metal contact area. Shot-peened craters were identified and distinguished from measured smaller-scale surface roughness before and after testing using an established numerical algorithm built on Matlab (16). Based on this analysis, a wear model was created to allow the correct prediction of surface roughness variation in repeated sliding.

2 Surface burnishing

2.1 Asperity plastic flattening

In the current peening stage of the manufacturing route of these components there are several important parameters that are not uniquely specified. Neither the length of time for which the surface is shot peened, nor the stand-off distance from which peening is performed, are specifically defined. These can vary depending on where, and by whom, the peening was done. Images from four samples surfaces peened with ceramic media and taken from pipe end sections produced at different times are compared in Fig. 3. These images were constructed using an Olympus LEXT 3D confocal microscope. After peening, the directional surface machining marks are no longer visible and the texture becomes almost isotropic which contrasts with a simply machined or plated specimen. Shot peened craters exhibit a random pattern that can be clearly seen on the surface images. The algorithm developed by Ahmed

and Sutcliffe (16) was applied to identify the areas of craters or pits and thus evaluate the proportion of the total area that they represent.

Figure 4 shows the distribution of the surface height data for the four samples with different R_a surface roughness values indicated in the legend. Note that the total number of pixels of each measurement is the same and the curves have been smoothened. In all cases the distribution is close to Gaussian or normal distribution indicating the random nature of the surface roughness. For the sample with the largest R_a there are a greater number of higher peaks and deeper troughs. This surface may well have been produced with larger peening media particles. Higher peaks imply more material movement and local deformation. In the case of the other samples, where the R_a surface roughness is approximately 2μm, the number of baseline height values is higher and the number of larger peaks and troughs reduced. When the value of the roughness is lower, the profile of the surface is more concentrated around the base line. Surface roughness is dependent on the shot peening media and shot peening time. Although samples were of different roughnesses, the area percentage of shot peened craters was similar, as shown in Fig. 3, which suggests that the pit percentage was independent of the surface roughness.

It is well established that when any rough surface is in contact with a rigid counterface, the area of "real" contact is only a small proportion of the nominal contact area (17). In order to simplify the application of a wear model, the surface asperities in the case here examined are regarded as having uniform amplitude and equal spacing. To represent a stochastic or random distribution of surface heights in a simplified manner, Christensen (18) introduced an asperity shape (shown in Fig. 5) whose height satisfies a Gaussian distribution of surface heights. The premise is that each individual asperity with Christensen profile would

provide the same relation between load and area as would be the case for a population of asperities of different heights with random distribution. This shape function was implemented in a MATLAB code which relates the ratio of the true contact area Λ to the remaining asperity height h and the initial r.m.s surface roughness described later in section 2.2. During a friction test (and in the make-up procedure) the peaks on the surface become worn thereby altering the characteristics of the surface, as illustrated by Fig. 5. The normal load carried by the surfaces in contact is shared between the asperities and the pressurised lubricant trapped in the troughs or valleys formed at the interface. In simple terms, we might write

$$\bar{p} = P_a \Lambda + P_v (1 - \Lambda) \tag{2}$$

where $\bar{p}$ is the mean pressure, P_a is the contact pressure between the asperities, P_v is the oil pressure in the valleys and Λ is the contact ratio, i.e. the proportion of the area represented by asperity contact. The initial contact pressures experienced on the peaks of the surface are significantly higher than the average contact pressure causing asperity plastic deformation. Initial flattening of asperity peaks is governed by plastic deformation so that the contact area can be solved from eqn. (2) as

$$\Lambda = \frac{\bar{p} - P_v}{P_a - P_v} \tag{3}$$

in which the value of P_a can be associated with, and so replaced by, the indentation hardness H_v.

The contact pressure is very high in premium tubular connections and so significant surface wear and asperity plastic deformation is expected. It is for this reason that Christensen surface asperity model is applied instead of the well-known Greenwood and Williamson

elastic model (19): it is unrealistic to assume the surface asperities all have constant radius and all deform elastically.

With the increase in contact ratio, further flattening of the asperities will occur governed by wear. We assume that the wear rate is determined by the asperity contact pressure P_a which can be found from eqn. (2) for given average contact pressure and lubricant pressure in the valleys,

$$P_a = \frac{\bar{p} - (1-\Lambda)P_v}{\Lambda} \tag{4}$$

Once wear and plastic flow has ceased so that elastic conditions are re-established, the average contact pressure might be derived from Hertzian contact theory applied to each asperity, so that

$$\bar{p} \approx \frac{1}{\pi} \times \left(\frac{16WE^{*1/2}}{9R^2} \right) \tag{5}$$

where W is the normal load acting on the surface, R is the reduced radius of contact and E^* is the contact modulus. Note that this is assuming the surface asperity flattening would not change the global contact area too much.

2.2 Lubricant entrapment and leakage

The effect of sliding friction test on the surface topography of the bronze plated surface and the shot-peened surface is shown in Fig. 6. The plated surface topography has changed from initial transverse lay to longitudinal due to the sliding. The craters on the shot-peened surface have been burnished leaving galling marks along the sliding direction. It is inferred from the evolution of the surface topography that the surface asperities are flattened as a result of local plastic deformation and abrasive wear. Simultaneously, most of the lubricant

trapped in the shot-peened craters has been removed through the porous contact interface as the normal load is ramped up during sliding. In these tests, sliding speeds are very low and the contact patch is small (~0.5mm as shown in Fig. 6b) so that it is expected that hydrodynamic effects will be insignificant. We can assume that the oil removal from the contact interface is thus dominated by the permeation through and around asperity contacts driven by the hydrostatic pressure gradient, as illustrated in Fig. 7.

Although more sophisticated models of lubricant flow within rough contact have been developed to account for large contact fractions (20, 21), we adopt the analysis of Patir and Cheng (22) who give the following set of equations to calculate the lubricant motion in the contact interface between two rough surfaces. For simplicity, the Couette effect is ignored, so that the lubricant flow rate q_x can be derived as

$$q_x = -\phi_x \frac{h_t^3}{12\eta} \frac{dP_v}{dx} \tag{6}$$

where ϕ_x and ϕ_s are respectively the pressure and shear flow factors, η is the oil viscosity, v is the sliding speed, h_t is the mean oil thickness, P_v is the valley lubricant pressure.

According to Wilson and his co-workers (21, 23), the flow factor for large fractional contacts can be calculated using the following equation for Christensen type asperities

$$\phi_x = \left[a_2 \left(H_t - H_{tc}\right)^2 + a_3 \left(H_t - H_{tc}\right)^3 \right] \Big/ H_t^3 \tag{7}$$

$$H_{tc} = 3\left| \left(1 - \left(0.47476/\gamma\right) + 1\right)^{-0.23007} \right| \tag{8}$$

$$a_2 = 0.051375\left(\ln 9\gamma\right)^3 - 0.0071901\left(\ln 9\gamma\right)^4 \tag{9}$$

$$a_3 = .0019 - 0.17927\ln\gamma + \left(0.047583\ln\gamma\right)^2 - \left(0.016417\ln\gamma\right)^3 \tag{10}$$

where γ is the Peklenik number which is defined as $\lambda_{0.5x}/\lambda_{0.5y}$ where $\lambda_{0.5x}$ and $\lambda_{0.5y}$ are the lengths at which the autocorrelation functions of the profile in the x and y directions reduce to 50% of their respective initial values and so identifies the roughness pattern of the surface. H_t is the ratio of the average film thickness h_t to r.m.s surface roughness R_q, and H_{tc} is the percolation threshold value of H_t. This is a measure of the remaining asperity height compared to initial surface height when the surface valleys are isolated. For a Christensen asperity, the normalised film thickness H_t and contact ratio Λ can be derived following, Patir and Cheng (24) and Lin et al (23), as

$$H_t = 3(35 + 128z + 140z^2 - 70z^4 + 28z^6 - 5z^8)/256 \tag{11}$$

$$\Lambda = \frac{16 - 35z + 35z^3 - 21z^5 + 5z^7}{32} \tag{12}$$

Where z is the normalised asperity height from baseline given by $z = h/y_0$ so that it varies between -1 and 1 and y0 is the initial asperity peak to valley hieght.

As a first approximation, the hydrostatic pressure gradient is assumed to be constant, i.e.

$$\frac{\mathrm{d}P_v}{\mathrm{d}x} = -\frac{P_v}{a} \tag{13}$$

where P_v is the hydrostatic pressure at the centre of the contact patch and a is the radius of contact. The flow rate per unit width through the contact edge can be derived by combining this equation with eqn (6) giving:

$$q_x = -\phi_x \frac{h_t^3}{12\eta} \frac{P_v}{a} \tag{14}$$

Therefore the reduction in lubricant volume in the contact patch due to leakage is given by:

$$\frac{dV}{dt} = 2\pi a q_x = \frac{\pi \phi_x h_t^3 P_v}{6\eta} \tag{15}$$

2.2 Asperity wear

Once any initial severe protuberances or surface spikes are plastically flattened, further asperity deformation is governed by asperity wear in sliding. The classic wear model due to Archard can be applied in which wear resistance is proportional to hardness (25). In particular

$$\frac{V}{s} = k \frac{F_N}{H} \tag{16}$$

where V is the wear volume, s the sliding distance and k a dimensionless wear rate which can be used as a fitting parameter in the program. F_N is the imposed normal load and H the hardness of the worn surface. This means that the wear volume is directly proportional to the normal force and inversely proportional to the hardness of the worn material, the peened surface in this case, because the counterface has a thick, harder bronze coating. Thus, if it can be assumed that it is the softer surface that wears, then eqn (16) can be rewritten as depth reduction rate viz.

$$\frac{dh}{dt} = k \frac{P_a}{H} v \ . \tag{17}$$

The volume reduction of the entrapped lubricant within the contact patch is also related to the reduction of asperity height due to wear and the pit area ratio described by eqn (17) giving:

$$\frac{dh}{dt} = \pi a^2 (1-\Lambda) k \frac{P_a}{H} \quad . \tag{18}$$

The average pressure in the valleys can then be derived by combining eqns. (15) and (18) to give

$$P_v = \frac{6\eta a^2 k v P_a (1-A)}{\phi_x H h_t^3} \tag{19}$$

As the sliding distance and the worn area increases, so the pressure in the valleys becomes more significant than was the case in the initial cycles. For the purposes of calculation, the proprietary lubricant used in the tests, was taken to have a viscosity of 50,000 cP (i.e. $50\,\mathrm{Pa\,s}$) as suggested by the manufacturer's data sheet.

It is thus possible to follow the history of the contact by using a sequential calculation. For an increment in sliding distance, first calculate $\bar{p}$ using eqn. (5) and P_v using eqn. (19). Then calculate P_a from eqn. (4) and the reduction in asperity height using eqn. (17). Update asperity height h and then contact ratio Λ and film thickness H_t using eqns. (11) and (12). Repeating this process for each increment of sliding distance yields the variation of asperity height h, asperity contact ratio Λ, valley pressure P_v and asperity contact pressure P_a for the whole sliding process.

Figure 8 shows the difference between the pressure on the asperities and the pressure in the valleys during the first cycle of the friction test. The valley pressure is much lower than asperity contact pressure at the beginning of the process but it becomes more significant as the oil pockets become isolated in subsequent cycles. A second consequence of wear is the reduction in asperity height and the increase in the contact ratio with sliding distance as

shown in Fig. 9. This comparison is for the first cycle both loading and unloading sections. As the sliding distance increases, the asperity height reduces and the contact ratio Λ, which is a measure of the area of contact between the two surfaces, also increases.

It can be noted that the hydrostatic pressure remains low until the conditions for percolation are reached in the second stroke: this leads to a rapid increase in lubricant pressure and a consequent decrease in asperity contact pressure. Hence the wear of asperities slows down. Strictly, the percolation threshold depends on the surface topography and thus on the Peklenik number (26): for a non-directional surface this has the value unity. The peened surface was initially non-directional and, although the plated surface had an initial roughness lay in which was transverse to the direction of sliding, it became longitudinal by wear marks as soon as sliding occurred. Consequently, a Peklenik number of 9 was assumed to reflect the longitudinal lay due to sliding. The initial value of the normalised R_q was less than unity because it is normalised by the combined initial roughness of the two faces in contact.

In order to produce a model that was comparable with the actual results obtained during the physical testing, a number of assumptions were made. The wear coefficient k used in the program was in the range of $1 \sim 4\text{x}10^{-4}$ which is in line with abrasive wear. The proprietary synthetic film lubricant had a viscosity of $50\,\text{Pa}\,\text{s}$, a value obtained from the manufacturer. In order to determine the value of the Eyring shear stress τ_0, properties of a lubricant with a similar viscosity were assumed. The surface roughness of the sample was measured using the techniques noted previously (section 2.1) prior to friction testing and at the end of each test for half cycle (one stroke), one cycle, 2 cycles and 3 cycles. This gave a series of surface roughness results at various sliding distances that could be compared with the outcome of the model. The area ratio on the plateau was obtained from the asperity wear

model results described in section 2. The effective contact radius was obtained from the size of the samples used in the friction tests. In this case, coupons with a radius of curvature of 60mm were used. The hardness value was obtained by nano-indentation testing. The hardness value of the softer material, a ceramic-peened surface, was used for the system because this was the surface which was burnished during sliding. The parameters for the model are summarised in Table 1.

For a wear coefficient k of $4x10^{-4}$, it is predicted that the shot-peened craters be removed within one cycle (c.f Fig. 9). This is in line with the observation on friction tests at 3mm/s. However the surface roughness of the shot-peened surface did not go to zero. This is owing to the galling of the plateaux. If this component is Rq0, the resultant surface roughness of the shot-peened surface can be derived as:

$$R'_q = \sqrt{R_q^2 + R_{q0}^2} \tag{20}$$

The theoretical predictions of surface roughness R_q' given by eqn (20) are compared with experimental measurements taken from samples prior to and after tests in Fig. 10 for a sliding speed of 3-15mm/s. Experimental measurements were taken from two separate tests with ceramic peened surface against plated surfaces under a load which increased linearly to 500 N as described previously (6). Surface measurements were taken after each stroke of sliding. The theoretical predictions are in good agreement with the experimental measurements suggesting that the model captures the main characteristics of the wear process. Surface burnishing occurs rapidly under typical contact conditions.

2.3 Friction model

The average frictional shear stress τ can be calculated by combining the shear stress acting on the plateaux and the shear stress of the lubricant within the valleys. This average

shear stress in the contact is calculated using eqn. (21), each stress is multiplied by the appropriate area ratio. Λ is the area ratio of the metal-to-metal contact and therefore $(1-\Lambda)$ is the area ratio of the thin film lubricant.

$$\tau = \Lambda\tau_a + (1-\Lambda)\tau_v \tag{21}$$

The ratio of asperity contact area Λ is determined by the lubricant film thickness and the surface roughness on the plateau which is given explicitly for each specific surface profile (27). The shear stress of the lubricant thin film is calculated using Eyring's equation (28):

$$\tau_v = \tau_0 \sinh\left(\frac{\eta v}{\tau_0 h_v}\right), \tag{22}$$

where τ_0 is the Erying shear stress of the lubricant, $\bar{p}$ is the mean contact pressure, h_v is derived from mean film thickness.

$$h_v = \frac{h_t}{1-\Lambda}, \tag{23}$$

where h_t is related to the remaining height of asperity described previously.

On the basis that the plateaux are boundary lubricated with ploughing, we can write that

$$\tau_a = (c + \tan\alpha)P_a, \tag{24}$$

where p_a is the pressure of the plateaux and c is the boundary friction factor and tan α is the slope of the asperities according to (11). The slope of the asperities is complicated due to the fact that two surfaces are combined but it can be associated with the combined surface roughness R_{qc} and the characteristic roughness spacing L.

$$\tan\alpha = \mathrm{m}.R_{qc}/L, \tag{25}$$

where m is the geometric factor, R_{qc} is the combined surface roughness, L is the characteristic asperity spacing.

$$R_{qc} = \sqrt{R_{q,1}^2 + R_{q,2}^2} \quad , \tag{26}$$

where $R_{q,1}$ and $R_{q,2}$ are the remaining r.m.s surface roughness of the shot-peened surface and the plated surface.

Finally the average coefficient of friction is given by:

$$CoF = \frac{\tau}{\bar{p}} \tag{27}$$

All the parameters applied are summarised in Table 1, and the results of the friction model are compared with experimental data in Fig. 11. The model prediction has been calculated using MATLAB and shows the relationship between the sliding distance and the coefficient of friction. It is shown that initially the CoF is approximately 20% higher than its final value. Within one stroke of sliding, the CoF decreases and stabilizes. In subsequent tests, the CoF is stable except a slight drop at the beginning of sliding. The graph shows two different sets experimental data, run at 15 mm/s with different samples. It is found that the final CoF fits the experimental data very well, but it decreases in the first stroke quicker than the prediction. It is believed that the short dwell at maximum load end where the sliding direction is reversed has accelerated lubricant leakage and burnishing of the surface.

3 Discussion and Conclusions

A classical wear model has been applied to the contact between a peened surface and a machined or plated surface to simulate the contact conditions in premium tubular connections. This was coupled with a simplified flow factor model for the side leakage of lubricant in the rough contact interface to predict the variation of lubricant pressure, the surface asperity height and hence the ratio of surface contact, with sliding distance. It was found that lubricant pressure was low until the contact percolation threshold was approached. The wear coefficient was regarded as fitting parameters. The model predictions of surface roughness fit the experimental measurements very well. The wear coefficient that best fits the experimental data was at the level of severe wear. This is in line with the observation of the variation of the surface topography.

In order to predict the coefficient of friction, a friction factor model was assumed to calculate the shear stress on the plateaux of the surface roughness. An overall coefficient of friction was derived using an average friction theory. Although there was uncertainty in the friction factor for 'real' metal-to-metal contact, the model predictions demonstrated the effect of surface burnishing on the overall friction. The trend was in agreement with experimental measurements of friction and the observations in the field. However, the experimental results showed that the reduction in friction occurs faster than model prediction. This is a simplified model with necessary assumptions regarding surface profile, the lubricant flow mechanism and the friction factor. To predict the friction more accurately would require a full 3D model of both hydrostatic and hydrodynamic flow of lubricant in the contact and a more accurate model of surface topography and boundary lubrication.

Acknowledgement

Financial support by Technology Strategy Board and Hunting Energy Services through a Knowledge Transfer Partnership is acknowledged. The authors would like to thank Andrew Leech, Alan Roberts, Bostjan Bensezek at Hunting Energy Services (UK) Ltd for constructive discussions during the course. The authors are grateful of the technical support of Terry Richards, Greg Nash at the School of Marine Science and Engineering of Plymouth University.

References

1. Bellarby J. Well Completion Design. Elsevier, editor. Amsterdam, The Netherlands: Elsevier; 2009.

2. Perrin D. Well Completion and Servicing. petrole Ifd, editor. Rueil-Malmaison, France1999.

3. Bradley AB, Nagasaku S, Verger E. Premium Connection Design, Testing and Installation for HPHT Sour Wells. SPE High Pressure-High Temperature Sour Well Design Applied Technology Workshop; 17-19 May; The Woodlands, Texas, USA2005. p. 1-8.

4. Kent S, Amiel G, Faucon B. North Sea Gas Leak Could Cost Billions. The Wall Street Journal. 2012.

5. Gosden E. Total's Elgin gas leak costing $2.5m a day. The Telegraph. 2012.

6. Stewart F, Le HR, Williams JA, Leech A, Bezensek B, Roberts A. Characterisation of friction and lubrication regimes in premium tubular connections. Tribology International. 2012;53:159 - 66.

7. Duggan TV. Applied engineering design and analysis. 1st Edition ed. London: Iliffe; 1969. 391 p.

8. API. API RP 7G - Recommended Practice for Drill Stem Design and Operation Limits 16th Edition. American Petroleum Institute,; 2009. p. 154.

9. API. API Test 5A3 3rd Edition; Recommended Practice on Thread Compounds for Casing, Tubing, Line Pipe, and Drill Stem; API Standards Catalogue. Englewood, Colorado, USA: American Petroleum Institute,; 2010. p. 210.

10. Carper HJ, Ertas A, Issa J, Cuvalci O. Effect of Some Material, Manufacturing, and Operating Variables on the Friction Coefficient in Octg Connections. J Tribol-T Asme. 1992;114(4):698-705.

11. Le HR, Sutcliffe MPF, Williams JA. Friction and material transfer in micro-scale sliding contact between aluminium alloy and steel. Tribol Lett. 2005;18(1):99-104.

12. Le HR, Williams JA, Luo JK. Characterisation of tribological behaviour of silicon and ceramic coatings under repeated sliding at micro-scale. Int J Surf Sci Eng.2(1-2): 1-13 2008.

13. Le HR, Sutcliffe MPF. Evolution of surface pits on stainless steel strip in cold rolling and strip drawing. J Tribol-T Asme. 2003;125(2):384-90.

14. Lo SW, Wilson WRD. A theoretical model of micro-pool lubrication in metal forming. Journal of Tribology. 1999;121:731-8.

15. Sutcliffe MPF, Le HR, Ahmed R. Modeling of micro-pit evolution in rolling or strip-drawing. Journal of Tribology. 2001;123:33-40.

16. Ahmed R, Sutcliffe MPF. Identification of surface features on cold-rolled stainless steel strip. Journal of Wear. 2000;244:60-70.

17. Persson BNJ. Elastoplastic Contact between Randomly Rough Surfaces. Physical Review Letters. 2001;87(11):116101-1 - -4.

18. Christensen H. Stochastic model for hydrodynamic lubrication of rough surfaces. Proceedings of the Institution of Mechanical Engineers. 1969-1970;184:1013-25.

19. Greenwood JA, Williamson JBP. Contact of Nominally Flat Surfaces. Proceedings of The Royal Society of Mathematical, Physical and Engineering Sciences. 1966;295:300-19.

20. Lo SW. A Study on Flow Phenomena in Mixed Lubrication Regime by Porous-Medium Model. J Tribol-T Asme. 1994;116(3):640-7.

21. Wilson WRD, Marsault N. Partial hydrodynamic lubrication with large fractional contact areas. J Tribol-T Asme. 1998;120(1):16-20.

22. Patir N, Cheng HS. Average Flow Model for Determining Effects of 3-Dimensional Roughness on Partial Hydrodynamic Lubrication. J Lubric Tech-T Asme. 1978;100(1):12-7.

23. Lin HS, Marsault N, Wilson WRD. A mixed lubrication model for gold strip rolling - Part I: Theoretical. Tribol T. 1998;41(3):317-26.

24. Patir N, Cheng HS. Application of Average Flow Model to Lubrication between Rough Sliding Surfaces. J Lubric Tech-T Asme. 1979;101(2):220-30.

25. Kwon DH, Park ES, Huh MY, Kim HJ, Cae JC. Wear behaviour of Fe-based bult metallic glass composites. Journal of Alloys and Compounds. 2011;509(1):105-8.

26. Li W-L, Chein W-T. Parameters for Roughness Pattern and Directionality. Tribology Letters. 2004;17(3):547-51.

27. Le HR, Sutcliffe MPF. Rolling of thin strip and foil: application of a tribological model for "mixed" lubrication. Journal of Tribology. 2002;124:129-36.

28. Sutcliffe MPF. Measurements of the Rheological Properties of a Kerosene Metal-Rolling Lubricant. P I Mech Eng B-J Eng. 1991;205(3):215-9.

Table 1 Parameters applied in the friction model

Parameter	**Value**
Contact modulus E^*	113GPa
Contact radius R	60 mm
Vickers hardness (peened surface) H_1	2.6 GPa
Vickers hardness (bronze plated surface) H_2	3.2Gpa
Initial surface roughness of peened sample $R_{q,1}$	2.8 μm
Initial surface roughness of bronze plated sample $R_{q,2}$	2.2 μm
Characteristic asperity half spacing L	50μm
Wear coefficient k	1~4x10^{-4}
Boundary friction factor in asperity contact c	0.12
Asperity geometric factor m	2.5
Eyring shear stress τ_0	2 MPa
Lubricant viscosity η	50 Pa s
Viscosity pressure index α	3.88×10^{-8} Pa^{-1}

Figure Captions

Fig. 1 Model of a premium pipe connection.

Fig. 2 Cross-cylinder friction and galling test rig setup: (a) schematic and (b) embodiment.

Fig. 3 Olympus LEXT surface height images of shot-peened steel samples.

Fig. 4 Height data distribution for 4 ceramic peened chrome steel samples.

Fig. 5 Normalised profile used to represent surface.

Fig. 6: Surface images after test (left) bronze-plate and (right) ceramic peened chrome steel.

Fig. 7 The overall contact patch is of radius a. Within this there will be a number of assumed circular individual asperity contact between which the oil must flow at rate q_x by permeation.

Fig. 8 Comparison of asperity and valley pressures for cycle 1 in simulated friction test, v=3mm/s, k=4x10^{-4}.

Fig. 9 Comparison of asperity height and contact area for cycle 1 in simulated friction test, v=3mm/s, k=4x10^{-4}.

Fig. 10 Comparison of model prediction (---) with experimental measurements

on sample 1 (□) at 3mm/s and sample 2 (x) at 15mm/s.

Fig. 11 Comparison of CoF model predictions (---) with experimental measurements(x, ◊, □) for sliding speed of 15 mm/s, c=0.12, m=2.5**,** k=1x10^{-4}

A Simplified Model of Surface Burnishing and Friction in Repeated Make-up Process of Premium Tubular Connections

H. R. Le[1]*, F. Stewart[2], J. A. Williams[3]

Figures

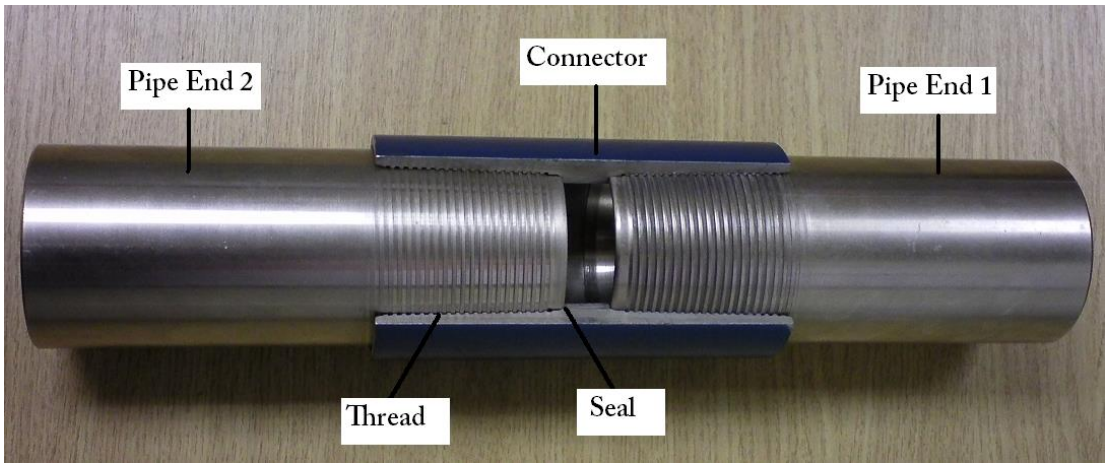

Fig. 1 Model of a premium pipe connection

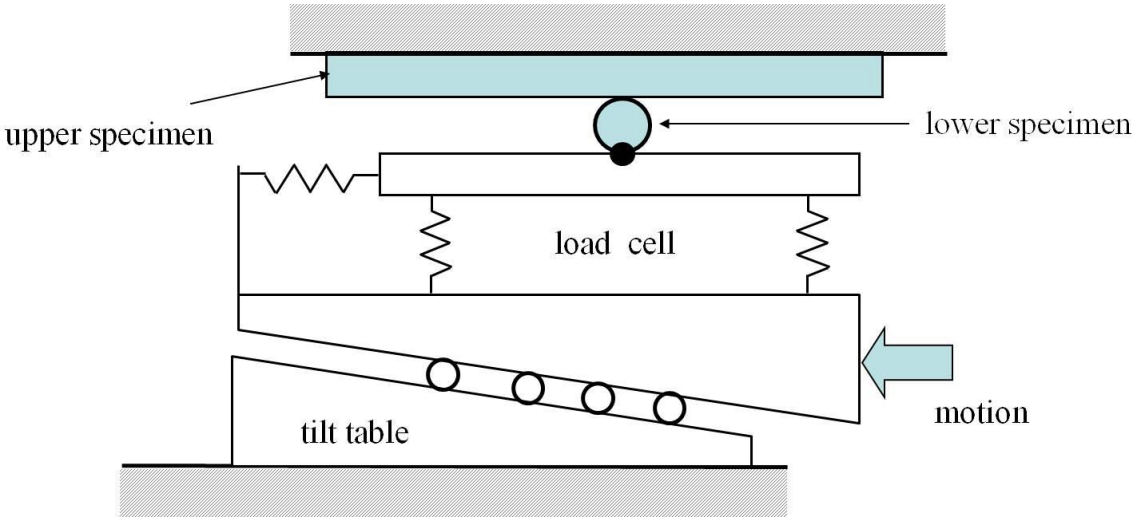

(a)

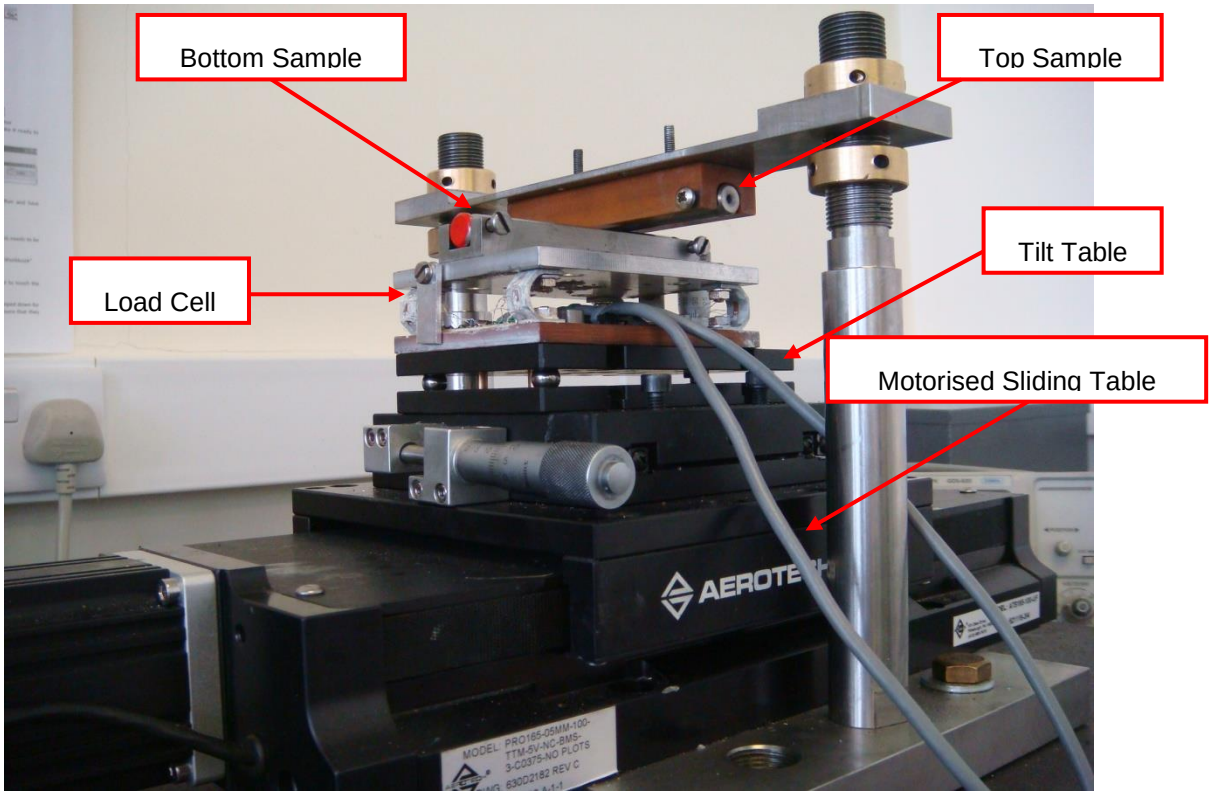

(b)

Fig. 2. Cross-cylinder friction and galling test rig setup: (a) schematic and (b) embodiment.

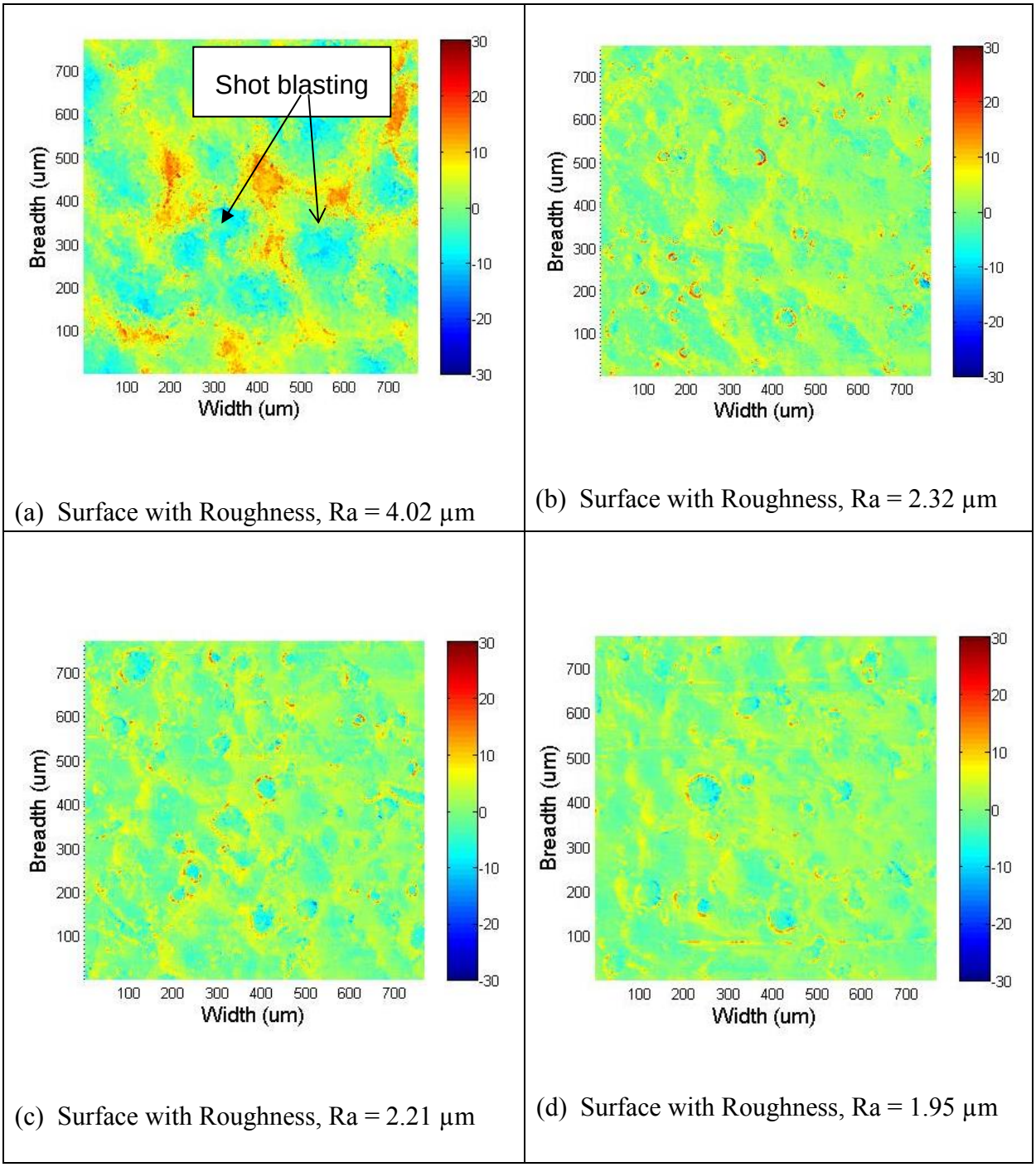

(a) Surface with Roughness, Ra = 4.02 µm

(b) Surface with Roughness, Ra = 2.32 µm

(c) Surface with Roughness, Ra = 2.21 µm

(d) Surface with Roughness, Ra = 1.95 µm

Fig. 3 Olympus LEXT surface height images of shot peened steel samples

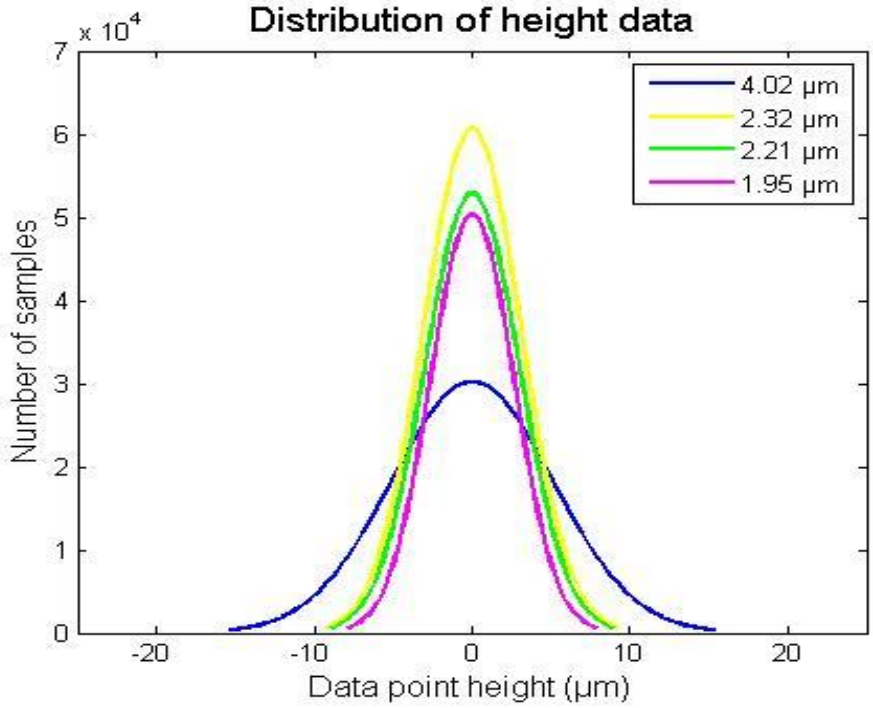

Fig. 4: Height data distribution for four ceramic peened chrome steel samples

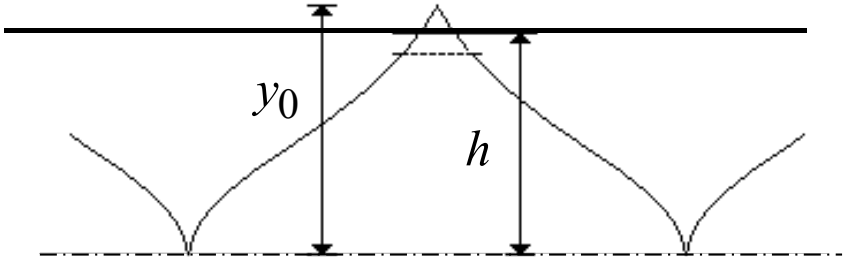

Fig. 5 Normalised profile used to represent surface

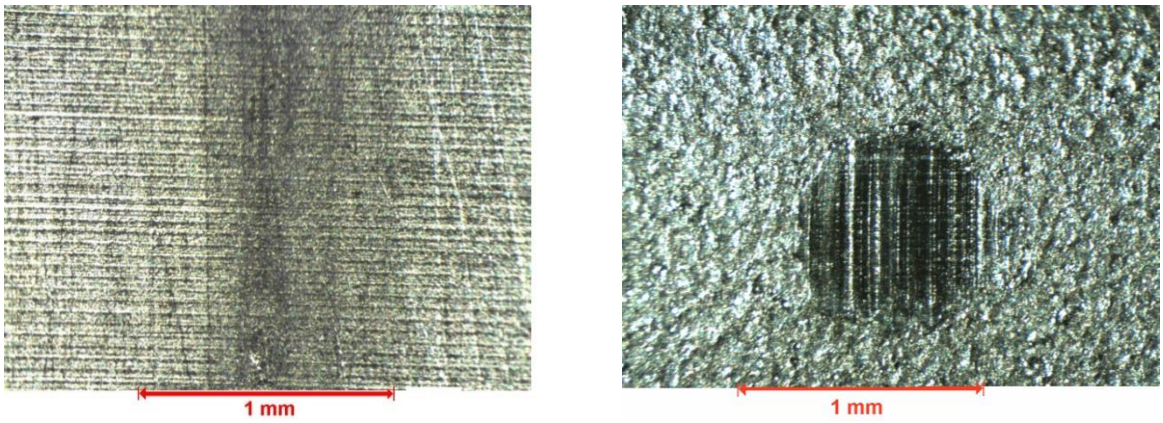

(a) (b)

Fig. 6: Surface images after test (a) bronze-plate and (b) ceramic peened chrome steel

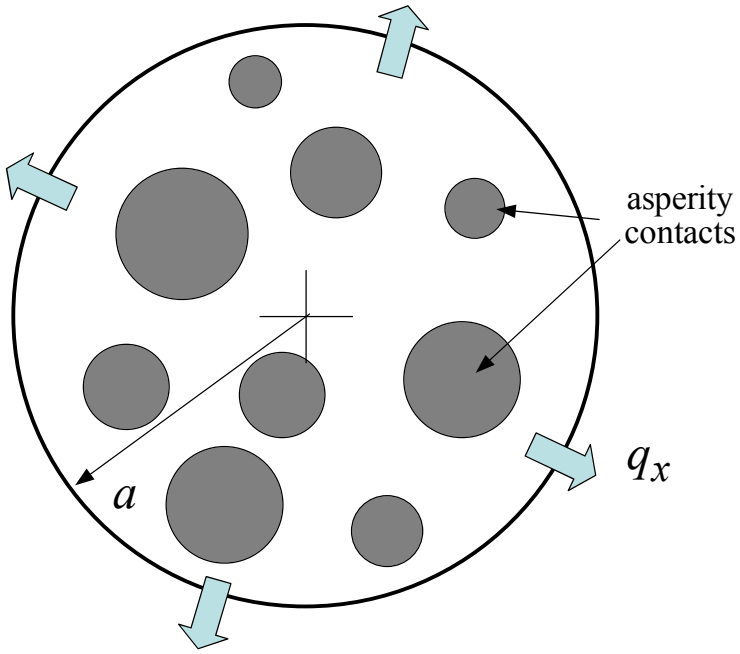

Fig. 7 The overall contact patch is of radius a. Within this there will be a number of assumed circular individual asperity contact between which the oil must flow at rate q_x by permeation.

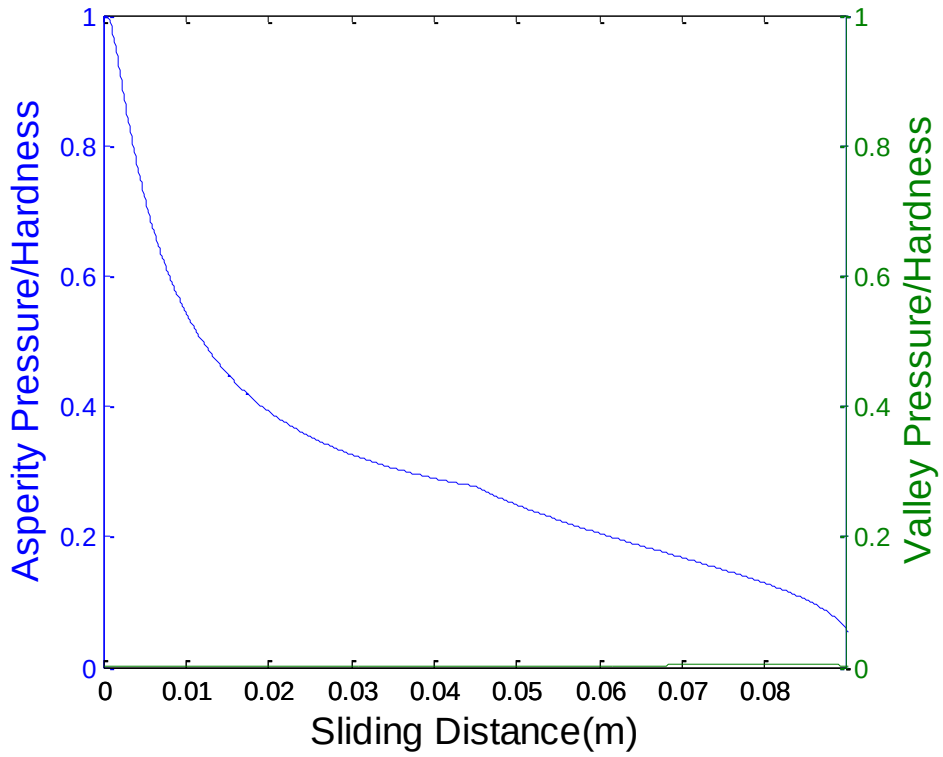

Fig. 8 Comparison of asperity and valley pressures for cycle 1 in simulated friction test, v=3mm/s, $k=4x10^{-4}$

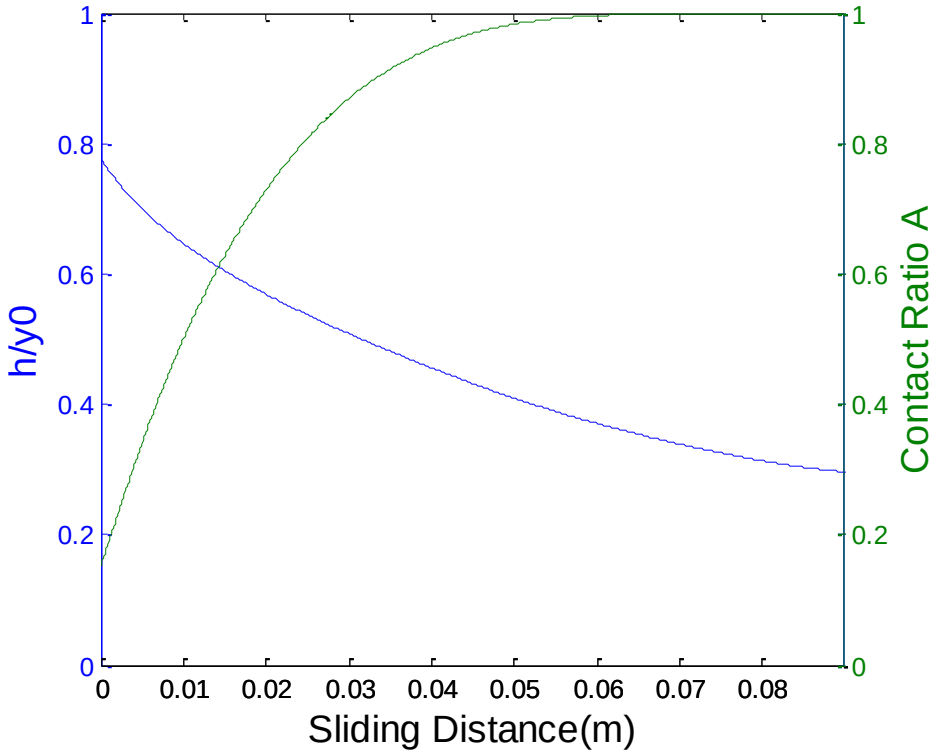

Fig. 9 Comparison of asperity height and contact area for cycle 1 in simulated friction test, v=3mm/s, $k=4x10^{-4}$

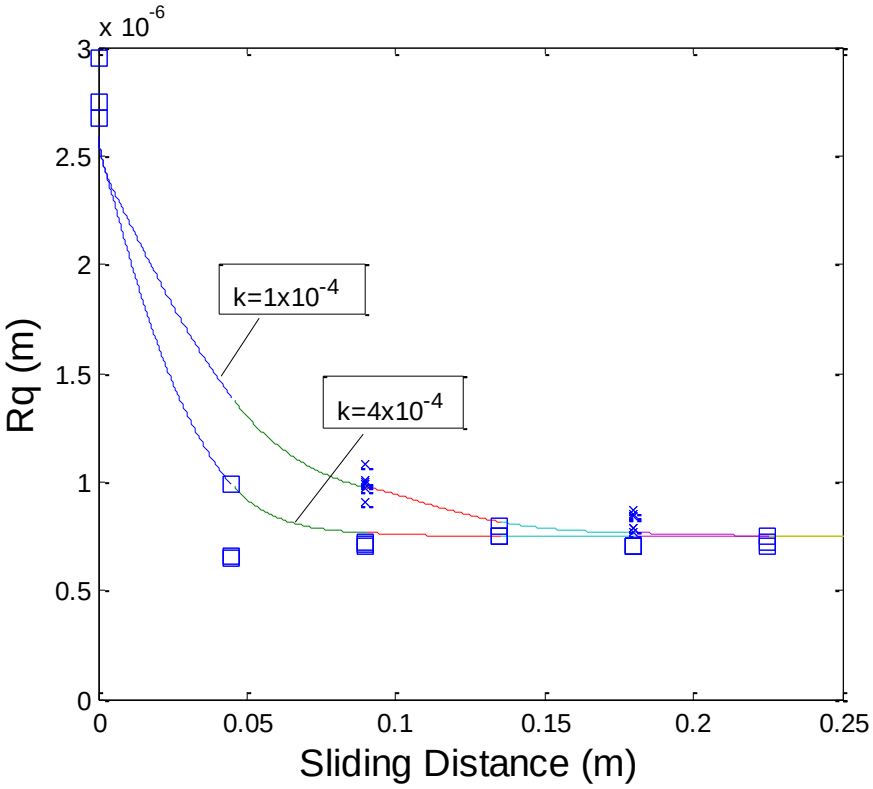

Fig. 10 Comparison of model prediction (---) with experimental measurements on sample 1 (□) at 3mm/s and sample 2 (x) at 15mm/s

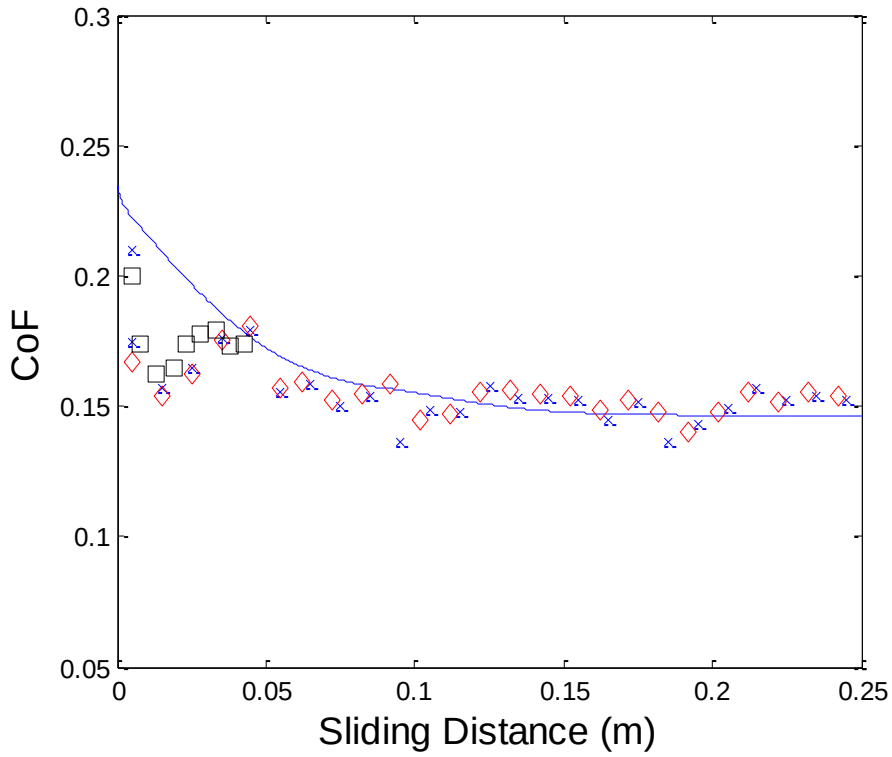

Fig. 11 Comparison of CoF model predictions (---) with experimental measurements(x, ◊, □) for sliding speed of 15 mm/s, c=0.12, m=2.5, k=1x10^{-4}